Reentrance of Berezinskii-Kosterlitz-Thouless-like transitions in three-state Potts antiferromagnetic thin film

Chengxiang Ding,[1,*] Wenan Guo,[2,†] and Youjin Deng[3,‡]

[1] *Department of Applied Physics, Anhui University of Technology, Maanshan 243002, China*
[2] *Physics Department, Beijing Normal University, Beijing 100875, China*
[3] *Hefei National Laboratory for Physical Sciences at Microscale, Department of Modern Physics, University of Science and Technology of China, Hefei, 230027, China*

(Dated: October 6, 2014)

Using Monte Carlo simulations and finite-size scaling, we study three-state Potts antiferromagnet on layered square lattice with two and four layers $L_z = 2$ and 4. As temperature decreases, the system develops quasi-long-range order via a Berezinskii-Kosterlitz-Thouless transition at finite temperature T_{c1}. For $L_z = 4$, as temperature is further lowered, a long-range order breaking the Z_6 symmetry develops at a second transition at $T_{c2} < T_{c1}$. The transition at T_{c2} is also Berezinskii-Kosterlitz-Thouless-like, but has magnetic critical exponent $\eta = 1/9$ instead of the conventional value $\eta = 1/4$. The emergent $U(1)$ symmetry is clearly demonstrated in the quasi-long-range ordered region $T_{c2} \le T \le T_{c1}$.

PACS numbers: 05.50.+q, 11.10.Kk, 64.60.Cn, 64.60.De

arXiv:1410.0822v1 [cond-mat.stat-mech] 3 Oct 2014

I. INTRODUCTION

The q-state Potts model[1,2] has been studied for long time in statistical physics. For the ferromagnetic Potts model, the symmetry of order parameter is simply determined by the Potts spins. The physics is now well understood, thanks to the hypothesis of universality. In contrast, for antiferromagnetic Potts (AFP) model, the order parameter is not only associated with the spins but also with the underlying lattice. Thus, one should study case by case.

The properties of the AFP model are often related to extensive ground-state degeneracy, which may be caused by frustration[3] or not[4–6]. The extensive degeneracy of ground states may lead to an "entropy-driven" finite-temperature phase transition. The phase transition is characterized by partial ordered phase at low temperature, which is ordered on a sublattice of the lattice, satisfying the minimum energy and maximum entropy by local modification of the spin states.

The three-state AFP model show good examples of such phase transitions. In three-dimensional simple-cubic lattice, when temperature is high, the model is disordered; when temperature is sufficiently low, some long-range order develops, and the following states could be favored: the spins on one of the sublattices are "frozen" at a random Potts value, and the spin on any site of the remaining lattice is "free" to take the other Potts values. In Refs. 7 and 8, such states are called "ideal" states. On the simple cubic lattice, there are six types of such ideal states. Thus, the order parameter is of the Z_6 symmetry. Monte Carlo simulations show that the model undergoes a continuous phase transition[9,10] between the high-temperature disordered phase and the low-temperature partial ordered phase which breaks the Z_6 symmetry. The critical exponents fall into the universality class of three-dimensional XY model[11].

In two dimensions, the three-state AFP model is extensively studied on different lattices. On the dice lattice[12], the model undergoes a continuous ordered-disordered phase transition at finite-temperature. which belongs to the universality of three-state ferromagnetic Potts model. On the honeycomb lattice[13], the model is disordered at any temperature, including the zero temperature. On the kagome lattice[14], the model is disordered at any nonzero temperature but critical at zero temperature. The magnetic critical exponent, governing the decay of two-point correlation function, is known to be $\eta = 4/3$. The phase diagram of the model on the square lattice is similar to that on the kagome lattice, but the critical exponent $\eta = 1/3$. However, when ferromagnetic next-nearest neighboring (NNN) interactions are included, the model has two Berezinskii-Kosterlitz-Thouless (BKT) transitions[15].

In this work, using a combination of various Monte Carlo algorithms, including the standard Metropolis method, the Wang-Swendsen-Koteký (WSK) cluster method[9] and the geometric cluster method[16–18], we study the three-state Potts antiferromagnet on the square lattice with multilayers, with antiferromagnetic interactions between layers. For the two-layer lattice, we find that the system undergoes a continuous phase transition at finite temperature $T_{c1} > 0$. The transition is of BKT type, which has magnetic exponent $\eta = 1/4$, different from $\eta = 1/3$ for the single-layer system at $T = 0$. In the whole low-temperature region $0 \le T \le T_{c1}$, the $L_z = 2$ system is quasi-long-rang ordered, with varying critical exponents η. As the number of layers is increased up to $L_z = 4$, we find that beside the BKT transition at T_{c1}, the system undergoes a second BKT phase transition at a lower temperature $T_{c2} < T_{c1}$, with critical exponent $\eta = 1/9$. When $T < T_{c2}$, a long-range order breaking the Z_6 symmetry develops. The emergent $U(1)$ symmetry is clearly demonstrated for the quasi-long-range ordered phase $T_{c2} \le T \le T_{c1}$.

The organization of the present paper is as follows. Section. II defines the model and the observables to be sampled, and introduces the algorithms used in our simulations. The simulation results, including the results for two-layer and four-layer square lattices, are given in Sec. III. We then finally conclude with a discussion in Sec. IV.

II. MODEL, ALGORITHM, AND OBSERVABLE

The three-state Potts model is defined by a simple Hamiltonian

$$\mathcal{H} = -K \sum_{\langle i,j \rangle} \delta_{\sigma_i,\sigma_j} \tag{1}$$

where the sum takes over all nearest neighboring sites $\langle i,j \rangle$. The spin assumes $\sigma_i = 1, 2, 3$, and $K = J/k_B T$ is a dimensionless coupling constant. The model is ferromagnetic when $J > 0$ or antiferromagnetic when $J < 0$. In the current paper, we focus on the antiferromagnetic case and set $J/k_B = -1$ for convenience.

The Potts spin σ can also be written as unit vector in the plane

$$\vec{\sigma} = (\cos\theta, \sin\theta), \tag{2}$$

where $\theta = 0, \pm 2\pi/3$ represents the angle of the spin. The Hamiltonian of the three-state Potts model becomes then

$$\mathcal{H} = -\frac{2}{3} K \sum_{\langle i,j \rangle} \cos(\theta_i - \theta_j) \ , \tag{3}$$

apart from a constant.

For Monte Carlo simulations of the three-state antiferromagnetic Potts model on the single-layer square lattice, the Wang-Swendsen-Kotekýy (WSK) algorithm[9] is efficient even at zero temperature. On the two-layer lattice, the algorithm still works but the efficiency drops. At the low temperatures of the four-layer square lattice, the efficiency drops so much that it becomes difficult to give reliable data for systems of moderate sizes. To overcome this problem, we implement the geometric cluster algorithm[16–18]. It is shown that a combination of the geometrical algorithm, the WSK algorithm and the Metropolis algorithm significantly improves the efficiency, which enables us to extensively simulate systems with linear size up to $L = 512$.

The sampled observables in our Monte Carlo simulations include the staggered magnetization $m_{\rm s}$, the staggered susceptibility χ_s, the uniform magnetization $m_{\rm u}$, the uniform susceptibility $\chi_{\rm u}$, and the specific heat $C_{\rm v}$, which are defined as

$$m_{\rm s} = \langle |\mathcal{M}_{\rm s}| \rangle, \tag{4}$$
$$\chi_{\rm s} = N \langle \mathcal{M}_{\rm s}^2 \rangle, \tag{5}$$
$$m_{\rm u} = \langle |\mathcal{M}_{\rm u}| \rangle \tag{6}$$
$$\chi_{\rm u} = N \langle \mathcal{M}_{\rm u}^2 \rangle, \tag{7}$$
$$C_{\rm v} = N(\langle \mathcal{E}^2 \rangle - \langle \mathcal{E} \rangle^2)/T^2, \tag{8}$$

with $\mathcal{M}_{\rm s}$, $\mathcal{M}_{\rm u}$, and $\mathcal{E}$ defined as

$$\mathcal{M}_{\rm s} = \frac{1}{N} \sum_{\vec{r}} (-1)^{x+y+z} \vec{\sigma}(\vec{r}), \tag{9}$$

$$\mathcal{M}_{\rm u} = \frac{1}{N} \sum_{\vec{r}} \vec{\sigma}(\vec{r}), \tag{10}$$

$$\mathcal{E} = \frac{1}{N} \sum_{\langle i,j \rangle} \delta_{\sigma_i,\sigma_j} \tag{11}$$

where $\vec{r} = (x, y, z)$ is the coordination, $N = L^2 \times L_z$ is the number of sites of the lattice. The staggered magnetization $m_{\rm s}$ can be conveniently used to probe the breaking of the Z_6 symmetry in the ordered phase.

We also sample the correlation length ξ on one sublattice of a given layer. Specifically, a layered square lattice is divided to two equivalent sublattices according to the parity of $x + y + z$, denoted by "sublattice A" and "sublattice B"; the z-th layer of sublattice A is denoted by A_z. The in-layer sublattice correlation length ξ is then defined as[8]

$$\xi = \frac{(\chi/F - 1)^{1/2}}{2\sqrt{\sum_{i=1}^{d} \sin^2(\frac{k_i}{2})}} \ , \tag{12}$$

where $\vec{k}$ is the "smallest wavevector" of the square lattice along the x direction–i.e., $\vec{k} \equiv (2\pi/L, 0)$. The in-layer sublattice susceptibility χ and the "structure factor" F are

$$\chi = \frac{1}{N} \langle \Big| \sum_{\vec{r} \text{ on } \mathrm{A_z}} \vec{\sigma}(\vec{r}) \Big|^2 \rangle, \tag{13}$$

$$F = \frac{1}{N} \langle \Big| \sum_{\vec{r} \text{ on } \mathrm{A_z}} e^{i\vec{k}\cdot\vec{r}} \vec{\sigma}(\vec{r}) \Big|^2 \rangle \ . \tag{14}$$

In a critical phase, quantity ξ/L assumes a universal value in the thermodynamic limit $L \to \infty$. In a disordered phase, correlation length ξ is finite and ξ/L drops to zero, while in an ordered phase, ξ/L diverges quickly since "structure factor" F vanishes rapidly. Thus, ξ/L is known to be very useful in locating the critical points of phase transitions.

III. RESULTS

In simulations of the three-state AFP model on multilayer square lattice, periodic boundary condition is used, including the z direction. The largest system size in the simulation is $L = 512$ and each data point is averaged over $5 \times 10^6 \sim 10^7$ samples.

A. Three-state AFP model on the two-layer square lattice

The left of Fig. 1 is an illustrative plot of $m_{\rm s}$ versus T for the two-layer three-state AFP model for a series of system sizes. The figure shows that in high temperature, the staggered magnetization converges to zero; in low temperature, the magnetization also decreases as the system size increases; however the finite-size scaling behavior in this region is obviously different to that in the high-temperature region. This is shown more clearly by the log-log plot of $m_{\rm s}$ versus L for given temperatures, as shown in the right of Fig. 1. We find that the magnetization $m_{\rm s}$ in the low temperatures can be described by

$$m_{\rm s} = L^{y_{\rm s}-d}(a + b_1/\ln L + b_2 L^{y_i}), \tag{15}$$

where $d = 2$ is the spatial dimension, and $y_{\rm s}$ is renormalization exponent of the staggered magnetic

field, which varies continuously with the temperature. $b_1/\ln L$ and $b_2 L^{y_i}$ are the correction-to scaling terms, with $y_i < 0$. a, b_1, and b_2 are unknown parameters.

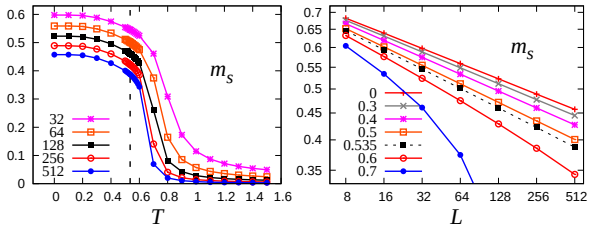

FIG. 1. (Color online) Left, staggered magnetization m_s versus T for the three-state AFP model on the two-layer square lattice; the dashed vertical line is set at the critical point $T_{c1} = 0.535$. Right, log-log plot of m_s versus L for given temperatures.

The meaning of the scaling behavior of m_s in the low-temperature region is twofold: First, it means that the staggered magnetization in the low-temperature region also converges to zero as the system size increases to infinite (because $y_s < 2$). This means that in the thermodynamic limit the Z_6 symmetry in the system is not broken, namely the system doesn't have long-range order on the sublattices. Second, it implies that this region is critical and the phase transition is of the BKT type. This result is confirmed by the behaviors of the staggered susceptibility. In the low temperatures, the staggered susceptibility scales as

$$\chi_s = L^{2y_s-d}(a + b_1/\ln L + b_2 L^{y_i}). \qquad (16)$$

The values of y_s at different temperatures can be obtained by fitting (15) or (16) to the data; the best estimations are listed in Table I.

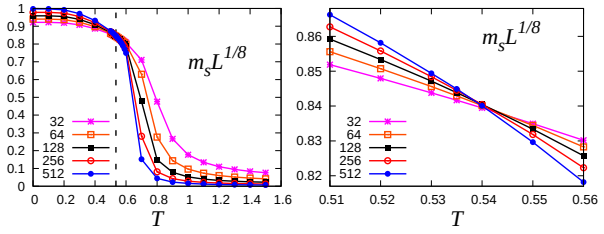

FIG. 2. (Color online) Left, plot of $m_s L^{1/8}$ versus T for various L. Right, an enlarge version of the left plot nearing the critical point. The dashed vertical line is set at the critical point $T_{c1} = 0.535$.

The critical point can be located more accurately by the finite-size scaling behavior of m_s. Figure 2 is a plot of $m_s L^{d-y_s}$ versus T, where we have set the value of y_s as the exact one for BKT transition, i.e., $y_s = 15/8$. It obviously indicates a transition at $T_{c1} \approx 0.54$. Fitting the data nearing this point by the following formula

$$m_s = L^{y_s-d}[a_0 + \sum_{k=1}^{2} a_k (T - T_{c1})^k (\ln L)^k + \sum_{j=1}^{2} b_j (T - T_{c1})^j + \frac{c_0}{\ln L} + c_1 L^{y_i}], \qquad (17)$$

we get $T_{c1} = 0.535(3)$. At this point, y_s is estimated to be 1.875(1), which coincides with the exact result 15/8. This gives a self-consistent check.

The uniform magnetization m_u and uniform susceptibility χ_u are also calculated in the simulations. It is found that m_u and χ_u show similar scaling behaviors as m_s and χ_s respectively, with the staggered exponent y_s replaced by a uniform exponent y_u. Doing similar fitting, y_u are obtained, which are also listed in Table I. Figure 3 is an illustrative plot of the critical exponents versus temperature T.

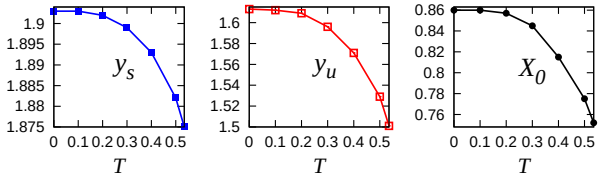

FIG. 3. (Color online) Critical exponents y_s, y_u and X_0 versus T for the three-state AFP model on the two-layer square lattice.

The BKT transition can also be demonstrated by the behavior of ξ/L, as shown in the left of Fig. 4. In the region $T > T_{c1}$, the value of ξ/L converges to zero as the system size increases; in the region $T \le T_{c1}$, the value of ξ/L converges to a finite nonzero value, which can be fit according to

$$\xi/L = X_0 + b_1/\ln L + b_2 L^{y_i} + \cdots, \qquad (18)$$

with $y_i < 0$. Table. I lists the results of X_0 for different temperatures.

In fitting the data according to Eqs. (15), (16), (17), and (18), the logarithmic terms are included. In fact, the BKT transition is characterized by logarithmic corrections[19–22], due to the presence of marginally relevant temperature field in renormalization[23].

TABLE I. Critical exponents of the three-state antiferromagnetic Potts model on the two-layer square lattice.

T	y_s	y_u	X_0
0.0	1.903(2)	1.613(2)	0.860(5)
0.1	1.903(2)	1.612(2)	0.860(5)
0.2	1.902(2)	1.609(2)	0.857(5)
0.3	1.899(2)	1.596(2)	0.845(5)
0.4	1.893(2)	1.571(2)	0.815(5)
0.5	1.882(2)	1.529(2)	0.775(5)
0.535	1.875(3)	1.501(3)	0.752(5)

At last, we present the result for the specific heat of the model, as shown in the right of Fig. 4. It is seen that the specific heat doesn't diverge but has a broad peak which converges to finite value. This is also the typical character of BKT transition.

B. The three-state AFP model on four-layer square lattice

On the four-layer square lattice, the three-state AFP model undergoes two BKT-like transitions,

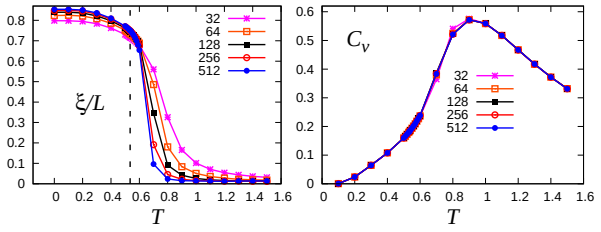

FIG. 4. (Color online) Plot of ξ/L and $C_{\rm v}$ versus T for various system sizes for the three-state AFP model on the two-layer square lattice; the dashed vertical line is set at the BKT point $T_{c1} = 0.535$.

which can be clearly demonstrated by the critical behavior of ξ/L, as shown in Fig. 5. At high temperature, the system is disordered and the value of ξ/L converges to zero as system size $L \to \infty$; at low temperature, the system is ordered which breaks the Z_6 symmetry and the value of ξ/L diverges; at the intermediate temperatures, the system is quasi-long-range ordered and the value of ξ/L converges to finite nonzero value X_0. By fitting the data according to (18), a series of X_0 are obtained and listed in Table II.

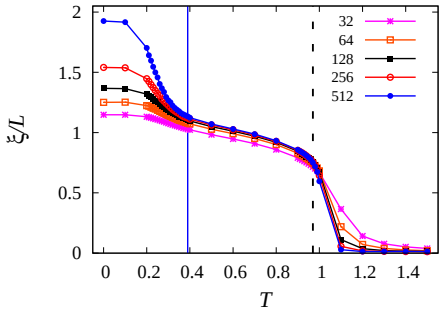

FIG. 5. (Color online) ξ/L versus T for the three-state AFP model on the four-layer square lattice. The dashed vertical line is set at $T_{c1} = 0.97$; the solid vertical line is set at $T_{c2} = 0.39$.

TABLE II. Critical exponents of the three-state antiferromagnetic Potts model on the four-layer square lattice.

T	$y_{\rm s}$	$y_{\rm u}$	X_0
0.39	1.944(2)	1.777(2)	1.15(1)
0.5	1.938(2)	1.752(2)	1.09(1)
0.6	1.933(2)	1.731(2)	1.04(1)
0.7	1.926(2)	1.704(2)	0.99(1)
0.8	1.917(2)	1.669(2)	0.93(1)
0.9	1.903(2)	1.612(2)	0.86(1)
0.97	1.874(3)	1.501(3)	0.75(1)

The two BKT-like transitions are further illustrated by the behavior of m_s in the left of Fig. 6. At high temperatures, the magnetization converges to zero as the system size increases; at low temperatures, it converges to nonzero value which indicates the break of Z_6 symmetry; in the intermediate temperatures, it scales as (15). The right of Fig. 6 is a log-log plot of m_s versus L for given temperatures, which shows the finite-size scaling behavior of m_s more clearly. The values of the critical exponent $y_{\rm s}$ in the quasi-LRO phase, obtained by fitting the data according to (15), are also listed in Table II. The fit is perfect in the region $0.39 \le T \le 0.97$ but deteriorates when $T < 0.97$ or $T > 0.39$; this implies the critical points $T_{c1} \approx 0.97$ and $T_{c2} \approx 0.39$.

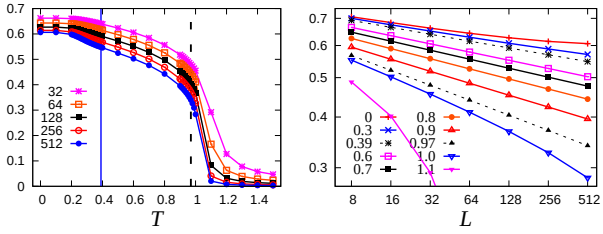

FIG. 6. (Color online) Left, m_s versus T for the three-state AFP model on the four-layer square lattice; the dashed vertical line is set at the BKT point $T_{c1} = 0.97$, the solid vertical line is set at the BKT point $T_{c2} = 0.39$. Right, log-log plot of m_s versus L for the three-state AFP model on the four-layer square lattice; the two dashed lines correspond to the BKT points.

Similar critical behaviors are observed for m_u and $\chi_{\rm u}$, the estimated values of $y_{\rm u}$ are listed in Table II. Figure 7 is an illustrative plot of the critical exponents versus temperature T.

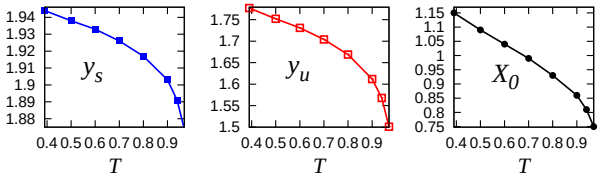

FIG. 7. (Color online) Critical exponents $y_{\rm s}$, $y_{\rm u}$ and X_0 versus T for the three-state AFP model on the four-layer square lattice.

The curve of the specific heat of the four-layer model is very similar to that of the two-layer model (right of Fig. 4); it has one and only one finite peak (but not diverge) at T_{c1}; it does not show any singularity.

The phase diagram of the three-state AFP model on the four-layer lattice is similar to that on the single-layer square lattice with ferromagnetic NNN interactions[15]. The latter can be mapped onto a Gaussian model, and the critical exponents $y_{\rm s}$ and $y_{\rm u}$ are determined by the vortex excitations in the Gaussian model with charge ± 1 and ± 2 respectively, with

$$y = 2 - \frac{n^2}{4\pi K_G}. \qquad (19)$$

Here $y = y_{\rm s}$ or $y_{\rm u}$, n is the charge; K_G is the coupling constant of the Gaussian model. For $T = T_{c1}$, $K_G = 2/\pi$, thus $y_{\rm s} = 15/8$ and $y_{\rm u} = 3/2$; for T_{c2}, $K_G = 9/2\pi$, thus $y_{\rm s} = 35/18$ and $y_{\rm u} = 16/9$. Assuming these results are also valid for the three-state AFP model on the multilayer lattice, we plot $m_s L^{d-y_{\rm s}}$ versus T with $y_{\rm s} = 15/8$ in the left of Fig. 8, which obviously shows the phase transition at T_{c1}. Fitting the data according

to (17) with $y_s = 15/8$ fixed, we obtained the critical point $T_{c1} = 0.967(5)$. The right of Fig. 8 is a plot of $m_s L^{d-y_s}$ versus T with $y_s = 35/18$, which obviously shows the phase transition at T_{c2}. A Similar fit yields $T_{c2} = 0.393(5)$.

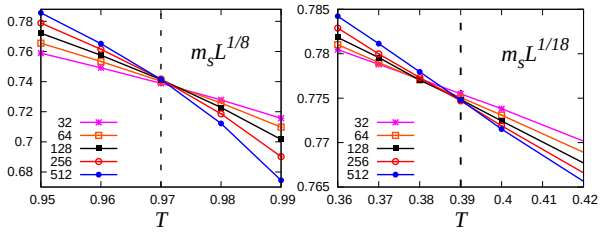

FIG. 8. (Color online) Plot of $m_s L^{y_s - d}$ versus T for the three-state AFP model on the four-layer square lattice. Left, $y_s = 15/8$; right, $y_s = 35/18$.

Furthermore, from Tables I and II we find that y_s and y_u satisfy

$$2 - y_u = 4(2 - y_s). \tag{20}$$

This is also the case for the three-state AFP model on the single-layer square lattice with ferromagnetic NNN interactions, which can be easily derived from Eq. (19).

We also calculate the observables concerning the rotational symmetry of the model

$$\phi_6 = \cos 6\theta \tag{21}$$

$$Q_\phi = \frac{\langle \phi_6^4 \rangle}{\langle \phi_6^2 \rangle^2}, \tag{22}$$

where θ is defined as the angle of the vector $\mathcal{M}_s$

$$\theta = \begin{cases} \tan^{-1}(\mathcal{M}_y/\mathcal{M}_x) + \pi/2, & \text{if } \mathcal{M}_x > 0 \\ \tan^{-1}(\mathcal{M}_y/\mathcal{M}_x) + 3\pi/2, & \text{if } \mathcal{M}_x < 0. \end{cases} \tag{23}$$

Here $\mathcal{M}_x, \mathcal{M}_y$ are the two components of $\mathcal{M}_s$. This definition makes the value of θ be in the region $[0, 2\pi]$. Q_ϕ is known to be useful in distinguishing the quasi-LRO phase and the true LRO phase[24].

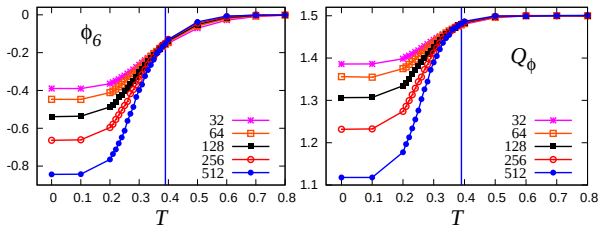

FIG. 9. (Color online) Plot of ϕ_6 and the Binder ratio Q_ϕ for the three-state AFP model on the four-layer square lattice. The vertical lines are set at the critical point $T_{c2} = 0.39$.

Figure 9 is the plot of ϕ_6 and Q_ϕ; it obviously indicates a phase transition at $T_{c2} \approx 0.39$. Figure 10 is the plot of the histogram of $(\mathcal{M}_x, \mathcal{M}_y)$. These results are easy to understand. In the the quasi-LRO phase m_s is zero in the thermodynamic limit, thus the angle of $\mathcal{M}_s$ can take random value in $[0, 2\pi]$; it is consistent with the emergent $U(1)$ symmetry of $\mathcal{M}_s$ in a finite

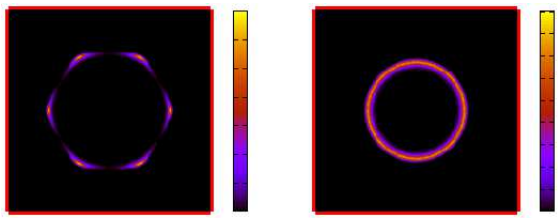

FIG. 10. (Color online) Histogram of $(\mathcal{M}_x, \mathcal{M}_y)$ for the three-state AFP model on the four-layer square lattice, with system size $L = 512$. Left, $T = 0.2$; right, $T = 0.7$.

system. In the low-temperature phase, m_s is not zero and the Z_6 symmetry is broken, the angle of $\mathcal{M}_s$ favors six directions in a finite system, as shown in the left of Fig. 10.

IV. CONCLUSION AND DISCUSSION

In conclusion, we have studied the three-state antiferromagnetic Potts model on the layered square lattice. On the two-layer lattice, the model undergoes a BKT-like transition at $T_{c1} = 0.535(3)$, with critical exponent $y_s = 15/8$ ($\eta = 1/4$). On the four-layer lattice, the model has two BKT-like transitions. One is between the high-temperature phase and the quasi-long-range ordered phase, with critical point $T_{c1} = 0.967(5)$ and critical exponent $y_s = 15/8$ ($\eta = 1/4$). Another one is between the quasi-long-range ordered phase and the low-temperature ordered phase which breaks the Z_6 symmetry, with critical point $T_{c2} = 0.393(5)$ and critical exponent $y_s = 35/18$ ($\eta = 1/9$). Emergent $U(1)$ symmetry is found in the quasi-long-range ordered phase.

The critical properties of the three-state AFP model on the square lattice are related to the vortex excitations, which is investigated by Kolafa[25] using Monte Carlo simulations. The simulations show that the positive and negative vortices are bound into dipoles only at the zero temperature; at any temperature $T > 0$, the dipoles unbind. There is no quasi-LRO phase in the single-layer AFP model. However, our simulations show that the multilayer structure can lead to a quasi-LRO phase. This is due to the modifications of the ground states by the layered structure. On a bipartite lattice such as the square lattice, the simple cubic lattice, or the layered square lattice, the density of entropy of the ideal states is $s_i = \ln 2/2 = 0.3466$. On the square lattice, the density of total entropy of the model is $s = 3/2 \ln(4/3)$[26]. The ratio is $r_s = s_i/s = 0.803$. On the simple cubic lattice $s = 0.367$ and $r_s = 0.945$. For the layered square lattice, although we have not numerically calculated its entropy density, we believe it is reasonable to postulate that the value of r_s is between 0.803 and 0.945; and it will gradually increase as the number of layers increases. The increase of r_s means the enhancement of the effect of ideal states, which will restrict the vortex excitations with nonzero charge, because the vortex excitations based on ideal states favor zero charge. As pointed out by Ref. 15, the

zero charge does not dominate the leading critical properties of the model. Therefore, comparing to the single-layer model, the multilayer model needs higher temperature to generate vortices with nonzero charge, thus the quasi-LRO phase of the two-layer model enters the region with $T > 0$. Another obvious result of the increase of r_s is the enhancement of the effect of Z_6 symmetry, which tends to make the system be ordered. However when the number of layers is two, the effect is not strong enough. When the number of layers increases to four, it is strong enough to lead to an ordered phase.

The phase diagram of the four-layer square-lattice AFP model is very similar to that of the single-layer square-lattice AFP model with ferromagnetic NNN interactions[15]. For the latter, the ferromagnetic NNN interactions have similar effect as that of the multilayer structure; it also enhances the Z_6 symmetry and restricts the vortex excitations with nonzero charge. However, the two model still have some subtle difference. For the single-layer model, if the ratio of the strength of the NNN interactions and the NN interactions takes fixed nonzero value, the system must be ordered at zero temperature. In such a case, it does not have a single BKT transition like that in the two-layer lattice. Furthermore, the entropy of the ground states of the single-layer model is not extensive; this is obviously different to that of the multilayer lattice, although it doesn't lead to substantial difference in critical behaviors.

For ferromagnetic model on multilayered lattice, the phase transition behavior belongs to the same universality class as that in the corresponding single-layer lattice[27–29], according to the hypothesis of universality. However, for antiferromagnetic model, due to the lattice structure dependence nature of the model, the number of layers may lead to substantially different behavior of phase transition from that in the corresponding single-layer lattice.

V. ACKNOWLEDGMENT

This work is supported by the National Science Foundation of China (NSFC) under Grant Nos. 11205005 (Ding), 11175018 (Guo), and 11275185 (Deng).

* dingcx@ahut.edu.cn
† waguo@bnu.edu.cn
‡ yjdeng@ustc.edu.cn

[1] R. B. Potts, Proc. Cambridge Phys. Soc. **48**, 106 (1952).
[2] F. Y. Wu, Rev. Mod. Phys. **54**, 235 (1982).
[3] A. Lipowski and T. Horiguchi, J. Phys. A **28**, 3371 (1995).
[4] N. G. Parsonage and L. A. K. Staveley, *Disorder in Crystals* (Oxford University Press, New York, 1978).
[5] Y. Deng, Y. Huang, J. L. Jacobsen, J. Salas, and A. D. Sokal, Phys. Rev. Lett. **107**, 150601 (2011).
[6] Q. N. Chen, M. P. Qin, J. Chen, Z. C. Wei, H. H. Zhao, B. Normand, and T. Xiang, Phys. Rev. Lett. **107**, 165701 (2011).
[7] J. Kondev and C. L. Henley, Nucl. Phys. B **464**, 540 (1996).
[8] J. Salas and A. D. Sokal, J. Stat. Phys. **92**, 729 (1998).
[9] J. S. Wang, R. H. Swendsen, and R. Kotecký, Phys. Rev. Lett. **63**, 109 (1989).
[10] J. S. Wang, R. H. Swendsen, and R. Kotecký, Phys. Rev. B **42**, 2465 (1990).
[11] Y.-H. Li and S. Teitel, Phys. Rev. B **40**, 9122 (1989).
[12] R. Kotecký, J. Salas, and A. D. Sokal, Phys. Rev. Lett. **101**, 030601 (2008).
[13] J. Salas, J. Phys. A: Math. Gen. **31**, 5969 (1998).
[14] D. A. Huse and A. D. Rutenberg, Phys. Rev. B **45**, 7536 (1992).
[15] M. P. M. den Nijs, M. P. Nightingale, and M. Schick, Phys. Rev. B **26**, 2490 (1982).
[16] C. Dress and W. Krauth, J. Phys. A **28**, L597 (1995).
[17] J. R. Heringa and H. W. J. Blöte, J. Phys. A **232**, 369 (1996).
[18] J. R. Heringa and H. W. J. Blöte, Phys. Rev. E **57**, 4976 (1998).
[19] R. Kenna and A. C. Irving, Phys. Lett. B **351**, 273 (1995).
[20] N. Schultka and E. Manousakis, Phys. Rev. B **49**, 12071 (1994).
[21] M. Hasenbusch, J. Phys. A **38**, 5869 (2005).
[22] A. Pelissetto and E. Vicari, Phys. Rev. E **87**, 032105 (2013).
[23] J. V. Jośe, L. P. Kadanoff, S. Kirkpatrick, and D. R. Nelson, Phys. Rev. B, **16**, 1217 (1977).
[24] S. K. Baek, P. Minnhagen, and B. J. Kim, Phys. Rev. E **80**, 060101(R) (2009).
[25] J. Kolafa, J. Phys. A: Math. Gen. **17**, L777 (1984).
[26] E. H. Lieb, Phys. Rev. **162**, 162 (1967).
[27] T. Mardani, B. Mirza, and M. Ghaemi, Phys. Rev. E **72**, 026127 (2005).
[28] Y. Asgari and M. Ghaemi, Physica A **387**, 1937 (2008).
[29] M. Ghaemi and S. Ahmadi, Physica A **391**, 2007 (2012).